Supplementary Information: Tunnel spectroscopy of localised electronic states in hexagonal boron nitride

SUPPLEMENTARY FIGURES

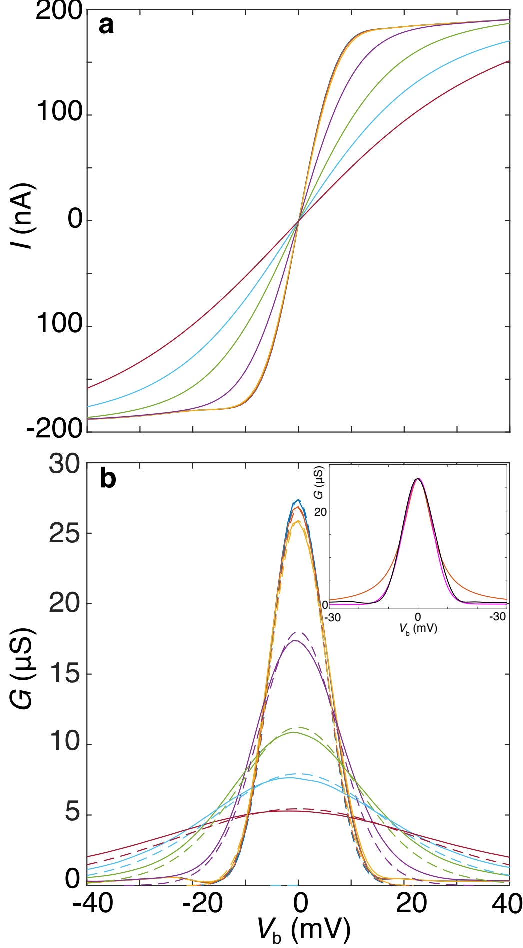

Supplementary Figure 1. Temperature dependence of electron tunnelling through state A when $T = 2$, 4, 6, 20, 40, 60, and 90 K. Solid curves in panels **a**, **b** show measured $I(V_b)$ and corresponding $G(V_b)$ characteristics. Dashed curves in **b** show $G(V_b)$ calculated using Eq. S4 for $\gamma = 6$ meV. Inset in **b** shows the lineshape of the peak in conductance measured when $T = 2$ K (black) and calculated using a Gaussian (magenta) and Lorentzian (brown) function for the density of states of the localised state.

SUPPLEMENTARY NOTES

Supplementary Note 1: Electrostatic Model

The electrostatic model used to determine the electrostatic configuration of Device 2, with a tunnel barrier width, d, bottom gate electrode thickness d_g^b and top gate thickness d_g^t, is given by

$$\begin{aligned} eV_b &= \mu_b - \mu_t - edF_b \\ eV_g^b &= \mu_b + ed_g^b F_g \\ eV_g^t &= \mu_b - ed_g^t F_t - edF_b. \end{aligned} \tag{S1}$$

where V_b, V_g^b and V_g^t are the bias, bottom gate and top gate voltages and μ_b and μ_t are the chemical potentials in the bottom and top electrodes measured with respect to the Dirac point in the respective layers. We calculate the electric fields within the bottom gate, F_g, top gate, F_t, and tunnel barrier regions, F_b, by solving these equations simultaneously using Gauss's law to determine the charge on the graphene layers. In Device 2 the bottom gate is a SiO_2 dielectric with a thin hBN capping layer with an overall dielectric constant which we set to be $\epsilon_g = 3.9$, the tunnel barrier and top gating electrode are hBN barriers which we set to have a dielectric constant of $\epsilon_b = 3.25$. We note that this model takes into account the quantum capacitance of the graphene layers. A similar set of equations can be obtained for Device 1. Further details of this model and its derivation can be found in Ref. [S1].

Supplementary Note 2: Landauer Büttiker Conductance

Here, we expand upon our analysis of tunnelling through a localised state using the Landauer Büttiker approach [S2–S4]. The current between the b and t electrodes and the localised state is given by

$$I_{b,t} = -e\gamma_{b,t}(f_{b,t} - N_o)/\hbar \tag{S2}$$

where $\gamma_{b,t}/\hbar$ is the electronic tunnelling rate from a localised state into the b and t electrodes respectively, $f_{b,t} = 1/(1 + \exp((E - \mu_{b,t})/k_B T))$ are the corresponding Fermi functions with temperature, T, and N_o is the occupancy of the defect state. Under steady state condition, the current between the graphene layers due to the impurity is $I_i = I_b = -I_t$ and thus

$$N_o = \frac{\gamma_b f_b + \gamma_t f_t}{\gamma_b + \gamma_t}. \tag{S3}$$

Assuming a finite energy broadening of the state $\gamma = \gamma_b + \gamma_t$, the total current through the impurity state is therefore given by

$$I_i = -\frac{e}{\hbar}\int_{-\infty}^{\infty} dE\ \Gamma(E - E_i)\frac{\gamma_b\gamma_t}{\gamma_b + \gamma_t}(f_b - f_t). \tag{S4}$$

where Γ is a singly peaked function with a full width half maximum (FWHM) of γ and $E_\mathrm{i} = E_\mathrm{i}^0 + eF_\mathrm{b}z_\mathrm{i}$. We set the parameters to correspond to state A, i.e. $E_\mathrm{i}^0 = E_\mathrm{A}^0 = 0.1$ eV and $z_\mathrm{i} = z_\mathrm{A} = 0.5d$, which give an accurate simulation of the X-shaped dependence of conductance in the measured colour map, compare Figs. 2**a** and **b** of the main text.

In Supplementary Figure 1 **a** we show $I(V_\mathrm{b})$ plots measured for $T = 2$ to 90 K with $V_\mathrm{g} = 1.7$ V so that $E_\mathrm{i} = \mu_\mathrm{b}$ when $V_\mathrm{b} = 0$ i.e. where the conductance loci cross in Fig.2**a**. In Supplementary Figure 1 **b** we show the measured differential conductance $G(V_\mathrm{b})$ curves (all solid) corresponding to the current voltage characteristics in **a**. As T increases the step-shaped increase in current broadens and the associated peak in the conductance weakens.

The dashed curves in Supplementary Figure 1 **b** show our calculated dependence of conductance on T around $V_\mathrm{b} = 0$, normalised to the peak conductance value of the measured data at $T = 2$ K. In this calculation, we define $\Gamma(E)$ to be a Gaussian function:

$$\Gamma(E) = \frac{1}{\sqrt{2\pi}\sigma} \exp\left(-\frac{E^2}{2\sigma^2}\right) \quad \text{(S5)}$$

where $\sigma = \gamma/2\sqrt{2\ln 2}$, and $\gamma = 6$ meV. We find very good correspondence between the calculation and the measured data, in particular the dependence on temperature of the lineshape, linewidth, and conductance peak height. To highlight the lineshape of the peak we show in the the inset of Supplementary Figure 1**b** a plot of $G(V_\mathrm{b})$ measured when $T = 2$ K (black) and calculated when $\Gamma(E)$ is a Gaussian function (magenta) and when $\Gamma(E)$ is a Lorentzian function (brown) when $\gamma = 6$ meV. Although both functions give a good fit to the data for small V_b, at larger V_b the measured conductance is quickly suppressed, consistent with the Gaussian lineshape (magenta) and diverges from the calculation when a Lorentzian is used. This lineshape is consistent with inhomogenous broadening of the level which could occur from spectral diffusion due to fluctuations in the electrostatic environment of the localised state [S5–S8].

We also make a quantitative analysis of the peak in the conductance. When $T = 0$ equation S4 becomes

$$I_\mathrm{i} = -\frac{e}{\hbar}\int_{\mu_\mathrm{b}}^{\mu_\mathrm{t}} dE\ \Gamma(E - E_\mathrm{i})\frac{\gamma_\mathrm{b}\gamma_\mathrm{t}}{\gamma_\mathrm{b} + \gamma_\mathrm{t}}. \quad \text{(S6)}$$

and therefore for small V_b

$$G_\mathrm{p} = \frac{e^2}{h}\beta \quad \text{(S7)}$$

where

$$\beta = \sqrt{\pi \ln 2}S \quad \text{(S8)}$$

and

$$S = 4\frac{\gamma_\mathrm{b}\gamma_\mathrm{t}}{(\gamma_\mathrm{b} + \gamma_\mathrm{t})^2} \quad \text{(S9)}$$

is the transmission probability of the channel. If $\gamma_\mathrm{b} = \gamma_\mathrm{t}$ and $\Gamma(E)$ is a Lorenztian function, then $G_\mathrm{p} = e^2/h$, corresponding the quantum of conductance. For state A, when $T = 2$ K, $G_\mathrm{p} = \beta e^2/h = 29$ μS, $\beta = 0.75$ and $S = 0.5$. Fermi's golden rule gives $\gamma_\mathrm{b,t} = 2\pi D_\mathrm{b,t}|\tau_\mathrm{b,t}|^2$ where $D_\mathrm{b,t} = 2E_\mathrm{b,t}A/\pi\hbar^2 v_\mathrm{F}^2$ is the density of states in the two electrodes, A is of the order of the area of the graphene lattice unit cell and $\tau_\mathrm{b,t} = \langle f|H|i\rangle$ is the tunnelling matrix element determined by the spatial overlap of the initial localised state and the final, extended, state in the graphene drain electrode. For $V_\mathrm{g} = 1.7$ V our electrostatic model gives $\mu_\mathrm{b} \sim 0.11$ eV and $\mu_\mathrm{t} \sim 0.09$ eV. Thus we deduce that $\gamma_\mathrm{b} > \gamma_\mathrm{t}$ and Eq. S7 suggests that the tunnel rates are $\gamma_\mathrm{b} \sim 0.8\gamma$ and $\gamma_\mathrm{t} \sim 0.2\gamma$. This difference cannot be explained fully by the difference in the density of states since $D_\mathrm{t}/D_\mathrm{b} \neq \gamma_\mathrm{t}/\gamma_\mathrm{b}$; this implies that the localised state is more strongly coupled to the bottom layer than the top i.e. $\tau_\mathrm{b} > \tau_\mathrm{t}$. We can estimate the tunnelling matrix element using Fermi's golden rule to obtain $|\tau_\mathrm{b}| = \hbar v_\mathrm{F}\sqrt{\gamma_\mathrm{b}/4A\mu_\mathrm{b}} \sim 0.2$ eV consistent with interlayer coupling in tight binding approximation of vdW heterostructures. Our analysis therefore indicates that tunnelling through the localised state is consistent with single electron tunnelling with different coupling amplitudes of the state with the top and bottom graphene electrodes.

Supplementary Note 3: Sequential Tunnelling

We model inelastic sequential tunnelling using the following equation

$$I_\mathrm{AB} = -\xi \int dE L_\mathrm{A}(E - E_\mathrm{A})\Gamma_\mathrm{B}(E - E_\mathrm{B}) \times \frac{\gamma_\mathrm{b}\gamma_\mathrm{AB}}{\gamma_\mathrm{b} + \gamma_\mathrm{AB}} f_\mathrm{t}(E)(1 - f_\mathrm{b}(E)), \quad \text{(S10)}$$

where $L_\mathrm{A}(E) = 1/(1 + \exp(-E/\sigma))$ is a step function with linewidth $\sigma = \gamma/2\sqrt{2\ln 2}$, and $\gamma = 6$ meV, i.e. corresponding to state A, Γ_B is the Gaussian density of states of localised state B and γ_AB is the tunnel rate between states A and B. The electron in the top graphene layer tunnels into state B with conservation of energy. Since state B is close to (or within) the top graphene layer we assume the tunnel rate between the top graphene layer and state B is much higher than γ_b and γ_AB. We set $\gamma_\mathrm{AB} = \gamma_\mathrm{t}$ which is a good approximation when state B is close to the top graphene layer. The step function then used to model the inelastic tunnelling process discussed in the main text, where the electron tunnels between states B and A by losing energy, i.e. the current can flow if $E_\mathrm{A} < E_\mathrm{B}$. The electron then tunnels into the bottom graphene layer. We include I_AB in our expression for the conductance and set the parameter, $\xi = 5$, to obtain a good fit of the amplitude of the sequential tunnelling feature to the measured conductance.

SUPPLEMENTARY REFERENCES

[S1] L. Britnell, *et al.*, *Science* **335**, 947 (2012).

[S2] Buttiker, M. Coherent and sequential tunneling in series barriers. *IBM J. Res. Dev.* **32**, 63-75 (1988).

[S3] Landauer, R. Spatial Variation of Currents and Fields Due to Localized Scatterers in Metallic Conduction. *IBM J. Res. Dev.* **1**, 223-231 (1957).

[S4] Datta, S, "Quantum Transport: Atom to Transistor", Cambridge 2005.

[S5] Sontheimer, B. et al. Photodynamics of quantum emitters in hexagonal boron nitride revealed by low-temperature spectroscopy. *Phys. Rev. B* **96**, 1-5 (2017).

[S6] Stoneham, A. M. Shapes of Inhomogeneously Broadened Resonance Lines in Solids. *Rev. Mod. Phys.* **41**, 82-108 (1969).

[S7] Wolters, J., Sadzak, N., Schell, A. W., Schröder, T. and Benson, O. Measurement of the ultrafast spectral diffusion of the optical transition of nitrogen vacancy centers in nano-size diamond using correlation interferometry. *Phys. Rev. Lett.* **110**, 1-5 (2013).

[S8] Neu, E. et al. Low-temperature investigations of single silicon vacancy colour centres in diamond. *New J. Phys.* **15**, (2013).